CHINESE OPTICS LETTERS

Vol. 19, No. 11 | November 2021

Switchable single- and dual-wavelength femtosecond mode-locked Er-doped fiber laser based on carboxyl-functionalized graphene oxide saturable absorber

Qimeng Lin (林启蒙)[1,2,3], Li Yan (闫 丽)[1,2,3], Yuanqi Song (宋园起)[1,2,3], Xuzhuo Jia (贾谞卓)[1,2,3], Xiaoqiang Feng (冯晓强)[1,2,3], Lei Hou (侯 磊)[1,2,3*], and Jintao Bai (白晋涛)[1,2,3**]

[1] State Key Laboratory of Energy Photon-technology in Western China, Shaanxi Engineering Technology Research Center for Solid State Lasers and Application, Northwest University, Xi'an 710069, China

[2] International Collaborative Center on Photoelectric Technology and Nano Functional Materials, Provincial Key Laboratory of Photo-electronic Technology, Northwest University, Xi'an 710069, China

[3] Institute of Photonics & Photon-technology, Northwest University, Xi'an 710069, China

*Corresponding author: lhou@nwu.edu.cn

**Corresponding author: baijt@nwu.edu.cn

Received July 5, 2021 | Accepted September 6, 2021 | Posted Online October 20, 2021

In this Letter, we demonstrated the switchable single- and dual-wavelength femtosecond soliton generation in single-mode Er-doped fiber lasers with the usage of carboxyl-functionalized graphene oxide (GO-COOH) saturable absorbers (SAs) for the first time, to the best of our knowledge. The fiber laser generated a stable single-wavelength conventional soliton at 1560.1 nm with a pulse duration of 548.1 fs. The dual-wavelength solitons centered at 1531.9 nm and 1555.2 nm with a spacing of approximately 23 nm can be obtained by adjusting the pump power of the cavity. Our experimental results indicated the GO-COOH has great potential to be used in ultrafast fiber lasers as broadband SAs.

Keywords: fiber laser; mode-locking; dual-wavelength; femtosecond soliton.

DOI: 10.3788/COL202119.111405

1. Introduction

The ultrashort pulse has potential widespread applications in optical communication, biomedical science, nonlinear optics, micromachining, etc[1–7]. The mode-locked fiber laser (MLFL) has attracted great attention due to its compact design and the ability to generate stable ultrashort pulses. Different types of soliton pulses and lots of nonlinear phenomena can be observed in the MLFLs with a proper parameter of the laser cavity, which is an ideal platform for researchers. However, there are many limitations in real applications because of the only single-output center wavelength of the MLFL, which is unable to satisfy some specific demands such as dense wavelength division multiplexing and dual-frequency comb. The emergence of dual-wavelength MLFL overcomes the drawback and further broadens the application range of the MLFL. Due to its unique advantages, the research interest for dual-wavelength MLFL is increasing day by day.

In order to obtain the stable dual-wavelength ultrashort pulse, different methods have been exploited with lots of effort from researchers. In the active MLFLs, birefringent polarization-maintaining fiber[8], dispersive cavity[9,10], optical filter[11–14], and highly nonlinear fiber (HNLF)[15] have been employed successfully for the generation of the dual-wavelength pulse output. Although the active MLFLs can achieve narrow linewidth and high repetition rate pulse output easily, the obvious disadvantages are broad pulse duration, increasing cost, and complexity of the system. In addition, more losses will inevitably be induced into the oscillator because of the inserted modulator. In contrast, the passive MLFLs are more suitable for the generation of the dual-wavelength ultrashort pulse. By virtue of a Lyot filter, an asynchronous dual-wavelength all-normal-dispersion MLFL was demonstrated at 1 μm[16]. An L-band wavelength-tunable and dual-wavelength MLFL was also achieved with the use of a hybrid structure of a no-core fiber and a graded-index multimode fiber at 1.5 μm[17]. In recent years, the emergence of two-dimensional (2D) nanomaterial enriches the dual-wavelength MLFLs, including bismuthene, black phosphorus (BPs), graphene, graphene oxide (GO), transition metal dichalcogenides (TMDs), carbon nanotubes (CNTs), topological insulators (TIs), and so on[18–32]. Compared with the methods mentioned above, the 2D nanomaterial is a better choice due to its simple and compact structure, low cost, and easy to achieve mode-locking operation.

Currently, a new type of 2D nanomaterial, carboxyl-functionalized GO (GO-COOH), has attracted the attention of many researchers. Its structure adds a carboxyl functional group to the GO that breaks the covalent bond. Its optical performance is similar to GO, but it also has unique properties. GO-COOH has strong hydrophilicity and very high solubility in water, which greatly simplifies the preparation process and reduces the manufacturing cost. The *Q*-switched and mode-locking pulse output in the Er-doped ring cavity was demonstrated based on the GO-COOH saturable absorber (SA) as the mode locker for the first time, to the best of our knowledge, where the mode-locking pulse repetition frequency was 22.7 MHz, and the pulse width was 1.5 ps[33]. The conventional soliton mode-locking with a pulse width of 500 fs at 1.5 μm was generated through a GO-COOH solution combined with a D-shaped fiber as the SA[34]. The *Q*-switched and femtosecond mode-locked pulse output at 1 μm was obtained successfully by using the GO-COOH SA. The mode-locking pulse repetition frequency was 22 MHz, and the pulse width was 239 fs after compression outside the cavity[35]. In previous work, the lasers worked in the single-wavelength conventional soliton mode-locking region with the GO-COOH SA at 1.5 μm, and there are no reports on the generation of femtosecond dual-wavelength soliton research.

In this Letter, we demonstrated the switchable single and dual-wavelength femtosecond soliton generation in a single-mode Er-doped fiber laser based on the GO-COOH SA. The switch only needed to adjust the pump power and polarization in the cavity. The modulation depth, saturable intensity, and unsaturated loss of the GO-COOH are 4.6%, 75.4 MW/cm^2, and 71.4%, respectively. The MLFL generated a stable single-wavelength soliton at 1560.1 nm with a pulse duration of 548.1 fs. The dual-wavelength solitons centered at 1531.9 nm and 1555.2 nm with a spacing of approximately 23 nm. The experimental results indicated that the GO-COOH is a promising candidate for dual-wavelength ultrashort pulse generation in a fiber laser.

2. Experimental Setup

The GO-COOH SA in our experiment was prepared by the liquid-phase-exfoliation method, and it was the same as that in Ref. [31]. A balanced twin-detector measurement method was used to investigate the nonlinear optical characteristics of the GO-COOH SA, and the configuration is displayed in Fig. 1(a). The seed source was a homemade 1.5 μm MLFL with a pulse repetition rate and a pulse width of 32 MHz and 586 fs, respectively. The input power was continuously adjusted through a variable attenuator, and the output power was recorded with a dual-channel power meter. The nonlinear transmission curve of the GO-COOH SA as a function of peak power intensity is shown in Fig. 1(b). The experimental data were fitted with a simplified two-level model as follows[17,36,37]:

$$T(I) = 1 - \Delta T \times \exp\left(-\frac{I}{I_{sat}}\right) - A_{ns}, \qquad (1)$$

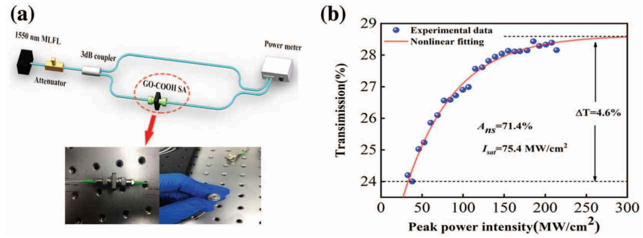

Fig. 1. (a) Setup of the balanced twin-detector measurement method; (b) nonlinear optical characteristics of the GO-COOH.

where ΔT, A_{ns}, and I_{sat} are the modulation depth, the non-saturable loss, and the saturation intensity, respectively. According to Eq. (1), the red fitting curve is illustrated in Fig. 1(b). The results indicated that the modulation depth of the GO-COOH SA was 4.6 %, and the saturation intensity was 75.4 MW/cm^2.

As shown in Fig. 2, the Raman spectrum of the GO-COOH SA was measured by a laser source centered at 532 nm. It is obvious with the two peaks in Fig. 2. The D peak was a result of the defect-induced breathing mode of sp^2 rings, and the G peak came from the double degenerate zone center E_{2g} mode, respectively. Compared with GO, the Raman spectrum indicates that GO-COOH has better structural symmetry.

The schematic of the GO-COOH SA femtosecond Er-doped MLFL is shown in Fig. 3. It was a typical ring cavity without dispersion management and was constructed with all-fiber components for a compact, alignment-free system. The pump source was a 980 nm laser diode with the maximum pump power of 550 mW and provided the energy to the Er-doped fiber through a 980/1550 nm wavelength division multiplexer (WDM). The length of the gain fiber was 60 cm, which has a group velocity dispersion (GVD) of $-23.5\ ps\cdot nm^{-1}\cdot km^{-1}$ (LIEKKI Er110-4/125). In order to ensure the unidirectional propagation, a polarization-dependent isolator (PD-ISO) was placed after the gain fiber. A polarization controller (PC) was used to adjust the birefringence. A 30% optical coupler (OC) was the only output port of the fiber laser to connect the measurement instruments. The GO-COOH SA was sandwiched with two patch cable connectors as a mode locker in the cavity. It was worth noting that the pigtails of all of the fiber components were standard single-mode fibers (SMFs),

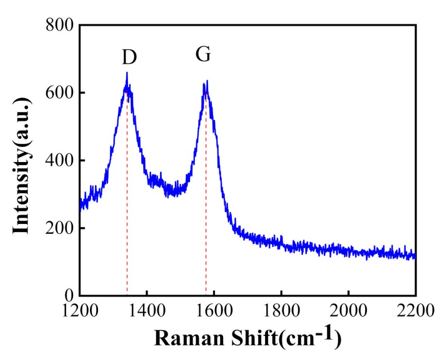

Fig. 2. Raman spectrum of GO-COOH film.

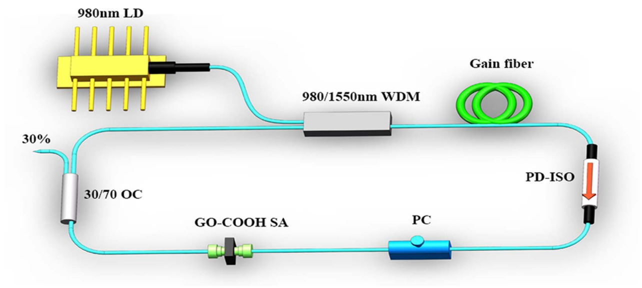

Fig. 3. Configuration of the Er-doped MLFL. WDM, wavelength division multiplexer; gain fiber, Er-doped fiber; PD-ISO, polarization-dependent isolator; PC, polarization controller; OC, optical coupler.

and the lengths of the SMF of the WDM, PD-ISO, OC, and SA were 2 m (including 1 m Hi1060 fiber), 2 m, 0.75 m, and 1.4 m, respectively. The total length of the cavity was 6.75 m, corresponding to a round-trip time of 32 ns, and the net dispersion was $-0.1\ \mathrm{ps}^2$. The measurement devices in our experiment were an optical autocorrelator (APE pulsecheck), a digital storage oscilloscope (Agilent DSO9104A) with a bandwidth of 1 GHz, and an optical spectrum analyzer (OSA, AQ6375B, Yokogawa Inc.) with a minimum resolution of about 0.02 nm.

3. Results and Discussion

With the increase of the pump power, and an appropriate adjustment of the polarization state through the PC, the stable MLFL could be established. The self-starting mode-locking threshold was about 50 mW. The performance of the output signal is illustrated in Fig. 4 at the pump power of 80 mW. Figure 4(a) displays the pulse train at different time scales. The oscilloscope trace indicated the time interval of the adjacent pulses was 32 ns, which matched well with the total length of the cavity. The inset was the pulse train at the 10 μs time scale, and there was no Q-switching phenomenon. Figure 4(b) was the optical spectrum of the output pulse. The center wavelength was 1560.1 nm with a full width at half-maximum (FWHM) of 5.1 nm. There were obvious sidebands in the envelope of the spectrum, which was the distinguishing feature of the conventional soliton. The radio frequency (RF) spectrum is shown in Fig. 4(c). The fundamental frequency was 31.2 MHz, and the signal-to-noise ratio (SNR) was 70 dB, which manifested a stable mode-locking operation. The inset was the RF spectrum at 1 GHz. The autocorrelation (AC) trace is depicted in Fig. 4(d). Assuming a hyperbolic secant shape, the pulse duration after nonlinear fitting was 548.1 fs.

With the further increase of the pump power, a new mode-locking state could be observed in the cavity. The threshold of the pump power was 450 mW, and a stable dual-wavelength mode-locking operation was established. The characteristics of the output pulse are displayed in Fig. 5. Figure 5(a) shows the periodical pulse train of laser emission. Compared with Fig. 4(a), it was clear that there were two solitons in the oscillator. The different pulse heights were caused by the different pulse energies of the two solitons. Meanwhile, these two solitons cannot be triggered at the same time. One soliton would move randomly when another soliton was fixed in the oscilloscope trace, which indicated that the GVD of the two solitons was different[38]. The envelope of the optical spectrum had changed greatly compared with Fig. 4(b). There were two peaks in the spectrum centered at 1555.2 nm and 1531.9 nm with a spacing of approximately 23 nm, and the FWHMs were 6.2 nm and 1.46 nm in Fig. 5(b), respectively. Kelly sidebands still could be observed in the spectrum, and the center wavelength had a blue-shift as the pump power increased. The RF spectrum with a scanning range of 40 kHz is illustrated in Fig. 5(c). There were

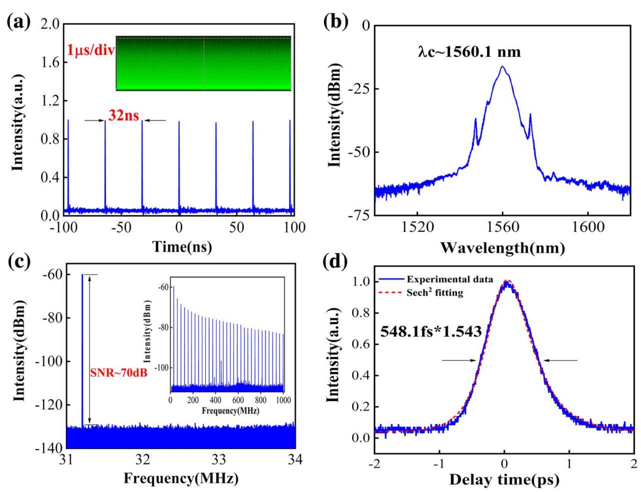

Fig. 4. Characteristics of single-wavelength conventional soliton fiber laser oscillator. (a) Oscilloscopic pulse train. (b) The corresponding optical spectrum. (c) Radio frequency (RF) spectrum; the inset is RF in the 1 GHz range. (d) Autocorrelation (AC) trace of the output pulse.

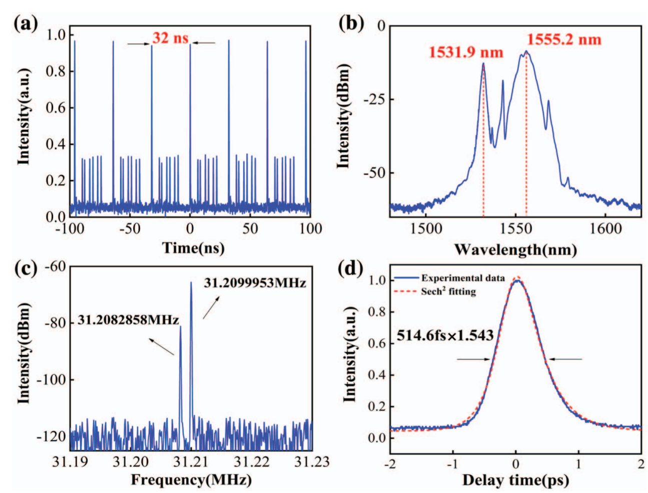

Fig. 5. Characteristics of dual-wavelength conventional soliton fiber laser oscillator. (a) Pulse train with different intensities. (b) The corresponding optical spectrum. (c) RF spectrum with 110 Hz resolution. (d) AC trace of the output pulse.

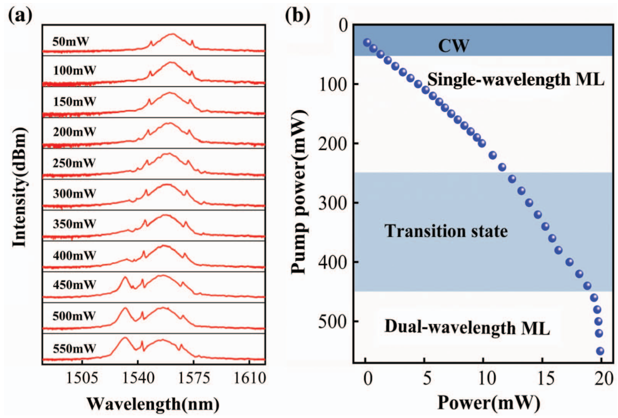

Fig. 6. (a) Evolution of the optical spectrum of the fiber laser with the pump power. (b) The evolution of the output power of the fiber laser with the pump power.

two peaks in the RF spectrum, and the difference in the repetition rate was 1709.5 Hz. This slight difference was due to the different GVD of pulses with different center wavelengths[17]. In theory, the relation could be described as follows[39,40]:

$$\Delta f = c^2 D\Delta\lambda / n^2 (L + LD\Delta\lambda c/n), \tag{2}$$

where Δf is the difference of the repetition rate, c is the speed of light, D is the dispersion parameter, $\Delta\lambda$ is the space of different center wavelengths, n is the index of fiber, and L is the total length. Here, $c = 3\times10^8\,\mathrm{m/s}$, $D_{\mathrm{SMF+EDF}} = 11.656\,\mathrm{ps/(nm\cdot km)}$, $L = 6.75\,\mathrm{m}$, $\Delta\lambda = 23.3\,\mathrm{nm}$, and $n = 1.46$. The Δf was 1698.8 Hz after calculation in theory based on the aforementioned parameters, and it matched well with the experimental result. Since there was no suitable bandpass filter centered at 1531.9 nm, only the AC trace of the pulse with a center wavelength of 1555.2 nm was measured in the experiment, and the result is depicted in Fig. 5(d). The pulse duration was 514.6 fs after nonlinear curve fitting.

The evolution of the output spectrum of the MLFL with the increasing pump power was also investigated, and the result is shown in Fig. 6(a). The stable mode-locking operation was established at the pump power of 50 mW, and it was obvious that the center wavelength of the spectrum had a continuous blue-shift from 1560.1 nm to 1555.2 nm. It could be found that the gain coefficient of the Er-doped fiber at 1531.9 nm increased gradually but was not enough to achieve dual-wavelength mode-locking at the pump power of 250–450 mW, and the laser was in a transitional state of single- and dual-wavelength mode-locking. When the pump power exceeded 450 mW, stable dual-wavelength mode-locking was obtained. The intensity of the peak at 1531.9 nm was larger than that at 1555.2 nm at the maximum of the pump power of 550 mW. This phenomenon could be attributed to the gain spectrum being modulated so that the gain coefficient at 1530 nm was greater than that at 1550 nm in the current case[40]. To verify that GO-COOH SA acted as a mode locker, the fiber laser cannot achieve self-starting mode-locking operation when the GO-COOH SA was only removed from the cavity. The experimental result indicated the GO-COOH SA played a dominant role in the fiber laser. Figure 6(b) shows the relationship between the pump power and the output power. The output power was linearly increased with the variation of the pump power. The average output power was 19.8 mW at the pump power of 550 mW, which was the

Table 1. Summary of the Dual-Wavelength Soliton Fiber Lasers Near 1550 nm with 2D Nanomaterials.

Nanomaterials	λ (nm)	$\Delta\lambda$ (nm)	Length of Gain Fiber (m)	Repetition Frequency (MHz)	Output Power (mW)	Pulse Duration (ps)	Ref. No.
Bismuthene	1531.6/1543.2	11.6	1.4	208	–	1.58	[18]
Bismuthene	1544.85/1554.53	9.68	1.4	44	–	–	[19]
Graphene	1533.4/1556.11	22.71	4.5	8.4/9.1	11.36	0.9/0.94	[20]
$Ti_3C_2T_x$-Mxene	1575.6/1587.5	11.9	1.3	11.1/166.5	–	–	[21]
G/SnO_2/PANI	1532/1557.6	25.6	5	2.13	3.2	1.25	[22]
$MnPS_3$	1565.19/1565.63	0.44	3.2	5.109	27.2	3800	[23]
WS_2	1568.55/1569	0.45	5	2.14	14.2	11	[24]
BP	1533/1558	25	3.2	20.8	–	0.7	[25]
h-BN	1531.5/1557.5	26	4.5	2.1	7.2	1.3	[26]
CNT	1531/1557	26	5	16.58	–	–	[27]
GO-COOH	1531.9/1555.2	23.3	0.6	31.2	19.8	0.515	This work

maximum output power that could be obtained in the MLFL based on the GO-COOH SA.

In our experiment, the switchable single- and dual-wavelength femtosecond soliton was observed without using the comb filter, which meant there was a birefringence-induced filter effect in the cavity. The gain spectrum was modulated by the birefringence-induced filter effect, which caused the two pulses at 1531.9 nm and 1555.2 nm to obtain different gains. The experimental results further proved that the birefringence-induced filter acted as a bandpass filter. As a result, the 1531.9 nm and 1555.2 nm wavelength bands were amplified, and the middle component was suppressed. It was worth noting that the switch of the single- and dual-wavelength mode-locking was reversible, and the pulse at 1531.9 nm will fade away with decreased pump power due to the saturable absorption effect[40]. Meanwhile, Table 1 summarizes the dual-wavelength soliton pulse output near 1550 nm by using different nanomaterials SAs from recent years[18–27]. It was clear that the performance of our fiber laser was excellent. Our work showed the great potential of GO-COOH SAs to achieve ultrashort pulse output in a dual-wavelength MLFL. In addition, we found the length of the gain fiber in our experiment was the shortest compared with previous related works. Generally speaking, the long gain fiber was suitable to achieve the dual-wavelength mode-locked operation. However, only the 0.6 m Er-doped fiber was adopted to search for dual-wavelength mode-locking in this work, and it could be obtained easily under a strong pump power. Maybe the experimental settings such as the dispersion, polarization, and pump power were more appropriate to the generation of the dual-wavelength pulse. The shorter gain fiber indicated that our fiber laser was cheaper and had more practical value in real applications.

4. Conclusion

In conclusion, the switchable single- and dual-wavelength femtosecond soliton was obtained in a single-mode Er-doped fiber laser with the usage of the GO-COOH SA for the first time, to the best of our knowledge. By properly adjusting the pump power, the single- and dual-wavelength femtosecond pulse could be achieved flexibly in the anomalous dispersion regime. The maximum output power was 19.8 mW. Our experimental results provided a possibility for the generation of the dual-wavelength femtosecond pulse in the Er-doped MLFL.

Acknowledgement

This work was supported by the National Natural Science Foundation of China (No. 11804276), the Natural Science Foundation of Shaanxi, China (No. 2019JQ-524), the Open Fund of State Key Laboratory of Transient Optics Photonics (No. SKLST201808), the Scientific Research Program Funded by Shaanxi Provincial Education Department (No. 17JS122), and the Open Fund of State Key Laboratory of Pulsed Power Laser Technology (No. SKL 2018KF01).

References

1. X. Fang, Z. Q. Wang, and L. Zhan, "Efficient generation of all-fiber femtosecond pulses at 1.7 μm via soliton self-frequency shift," Opt. Eng. **56**, 046107 (2017).
2. J. Luan, P. S. Russell, and D. Novoa, "Efficient self-compression of ultrashort near-UV pulses in air-filled hollow-core photonic crystal fibers," Opt. Express **29**, 13787 (2021).
3. A. Zemaitis, M. Gaidys, P. Gecys, M. Barkauskas, and M. Gedvilas, "Femtosecond laser ablation by bibursts in the MHz and GHz pulse repetition rates," Opt. Express **29**, 7641 (2021).
4. F. T. Zhang, X. H. Xie, X. J. Zhao, L. Ma, L. Lei, J. R. Qiu, and Z. G. Nie, "Polarization-dependent microstructural evolution induced by a femtosecond laser in an aluminosilicate glass," Opt. Express **29**, 10265 (2021).
5. K. Guesmi, L. Abdeladim, S. Tozer, P. Mahou, T. Kumamoto, K. Jurkus, P. Rigaud, K. Loulier, N. Dray, P. Georges, M. Hanna, J. Livet, W. Supatto, E. Beaurepaire, and F. Druon, "Dual-color deep-tissue threephoton microscopy with a multiband infrared laser," Light Sci. Appl. **7**, 12 (2018).
6. F. Akhoundi, Y. K. Qin, N. Peyghambarian, J. K. Barton, and K. Kieu, "Compact fiber-based multi-photon endoscope working at 1700 nm," Biomed. Opt. Express **9**, 2326 (2018).
7. D. Y. Shen, J. Qian, C. W. Wang, G. D. Wang, X. H. Wang, and Q. Z. Zhao, "Facile preparation of silver nanoparticles in bulk silicate glass by high-repetition-rate picosecond laser pulses," Chin. Opt. Lett. **19**, 011901 (2021).
8. J. B. Schlager and S. Kawanishi, "Dual wavelength pulse generation using mode-locked erbium-doped fiber ring laser," Electron. Lett. **27**, 2072 (1991).
9. S. L. Pan and C. Y. Lou, "Stable multiwavelength dispersion-tuned actively mode-locked erbium-doped fiber ring laser using nonlinear polarization rotation," IEEE Photon. Technol. Lett. **18**, 1451 (2006).
10. S. P. Li and K. T. Chan, "Electrical wavelength tunable and multiwavelength actively mode-locked fiber ring laser," Appl. Phys. Lett. **72**, 1954 (1998).
11. S. P. Li and K. T. Chan, "A novel configuration for multiwavelength actively mode-locked fiber lasers using cascaded fiber Bragg gratings," IEEE Photon. Technol. Lett. **11**, 179 (1999).
12. B. Bakhshi and P. A. Andrekson, "Dual-wavelength 10-GHz actively mode-locked erbium fiber laser," IEEE Photon. Technol. Lett. **11**, 1387 (1999).
13. G. E. Town, L. Chen, and P. W. E. Smith, "Dual wavelength modelocked fiber laser," IEEE Photon. Technol. Lett. **12**, 1459 (2000).
14. Z. H. Li, C. Y. Lou, Y. Gao, and K. T. Chan, "Dual-wavelength and dual-repetition-rate actively mode-locked fiber ring laser," Opt. Commun. **185**, 381 (2000).
15. Z. Chen, H. Z. Sun, S. Z. Ma, and N. K. Dutta, "Dual-wavelength mode-locked erbium-doped fiber ring laser using highly nonlinear fiber," IEEE Photon. Technol. Lett. **20**, 2066 (2008).
16. Z. R. Guo, Q. Hao, K. Huang, and H. P. Zeng, "All-normal-dispersion mode-locked fiber laser with a tunable angle-spliced polarization-maintaining fiber lyot filter," IEEE Photon. J. **13**, 1501108 (2021).
17. L. J. Li, Z. K. Wang, D. N. Wang, and F. Yang, "L-band tunable and dual-wavelength mode-locked fiber laser with NCF-GIMF-based SA," IEEE Photon. Technol. Lett. **31**, 647 (2019).
18. W. Xu, P. Guo, X. Li, Z. Hui, Y. Wang, Z. Shi, and Y. Shu, "Sheet-structured bismuthene for near-infrared dual-wavelength harmonic mode-locking," Nanotechnology **31**, 225209 (2020).
19. P. Guo, X. Li, T. Feng, Y. Zhang, and W. Xu, "Few-layer bismuthene for coexistence of harmonic and dual wavelength in a mode-locked fiber laser," ACS Appl. Mater. Inter. **12**, 31757 (2020).
20. K. Y. Lau, M. H. Abu Bakar, F. D. Muhammad, A. A. Latif, M. F. Omar, Z. Yusoff, and M. A. Mahdi, "Dual-wavelength, mode-locked erbium-doped fiber laser employing a graphene/polymethyl-methacrylate saturable absorber," Opt. Express **26**, 12790 (2018).
21. X. X. Yan, M. Jiang, E. K. Li, X. Kang, Z. Y. Ren, D. D. Li, T. Q. Wang, and B. L. Lu, "Tunable high-order harmonic and dual-wavelength mode-locking in Er-doped fiber laser based on $Ti_3C_2T_x$-Mxene," Appl. Phys. Express **14**, 012009 (2021).
22. B. Guo, Q. Y. Ouyang, S. Li, Z. J. Fang, and P. F. Wang, "Dual-wavelength soliton laser based on graphene ternary composite," Chin. J. Lasers **44**, 0703012 (2017).

23. Q. Yu, K. Guo, J. Chen, T. Wang, J. Wang, X. Y. Shi, J. Wu, K. Zhang, and P. Zhou, "Dual-wavelength self-starting mode-locking Er-doped fiber laser with $MnPS_3$ saturable absorber," Acta Phys. Sin. **69**, 184208 (2020).
24. B. Guo, S. Li, Y. X. Fan, and P. F. Wang, "Versatile soliton emission from a WS_2 mode-locked fiber laser," Opt. Commum. **406**, 66 (2018).
25. L. Yun, "Black phosphorus saturable absorber for dual-wavelength polarization-locked vector soliton generation," Opt. Express **25**, 32380 (2017).
26. B. Guo, S. Li, K. Zhang, Y. X. Fan, Z. J. Fang, J. Ren, L. B. Yuan, and P. F. Wang, "Hexagonal boron nitride: a rising nonlinear optical material for dual-wavelength soliton generation," chinaXiv:201611.00719 (2017).
27. C. Zeng, Y. D. Cui, and J. Guo, "Observation of dual-wavelength solitons and bound states in a nanotube/microfiber mode-locking fiber laser," Opt. Commun. **347**, 44 (2015).
28. B. Guo, Y. Yao, Y. F. Yang, Y. J. Yuan, L. Jin, B. Yan, and J. Y. Zhang, "Dual-wavelength rectangular pulse erbium-doped fiber laser based on topological insulator saturable absorber," Photon. Res. **3**, 94 (2015).
29. M. Liu, N. Zhao, H. Liu, X. W. Zheng, A. P. Luo, Z. C. Luo, W. C. Xu, C. J. Zhao, H. Zhang, and S. C. Wen, "Dual-wavelength harmonically mode-locked fiber laser with topological insulator saturable absorber," IEEE Photon. Technol. Lett. **26**, 983 (2014).
30. Y. C. Kong, H. R. Yang, W. L. Li, and G. W. Chen, "Switchable dual-wavelength all-fiber laser mode-locked by carbon nanotubes," Laser Phys. **25**, 015101 (2014).
31. X. Zhao, Z. Zheng, L. Liu, Y. Liu, Y. Jiang, X. Yang, and J. Zhu, "Switchable, dual-wavelength passively modelocked ultrafast fiber laser based on a single-wall carbon nanotube modelocker and intracavity loss tuning," Opt. Express **19**, 1168 (2011).
32. K. Y. Lau, P. J. Ker, A. F. Abas, M. T. Alresheedi, and M. A. Mahdi, "Mode-locked fiber laser in the C-band region for dual-wavelength ultrashort pulses emission using a carbon nanotube saturable absorber," Chin. Opt. Lett. **17**, 051401 (2019).
33. F. Y. Zhao, Y. S. Wang, Y. G. Wang, H. S. Wang, and Y. J. Cai, "Graphene oxide-COOH as a new saturable absorber for both *Q*-switching and mode-locking fiber lasers," Chin. Opt. Lett **15**, 101402 (2018).
34. R. D. Lv, L. Li, Y. G. Wang, Z. D. Chen, S. C. Liu, X. Wang, J. Wang, and Y. F. Li, "Carboxyl graphene oxide solution saturable absorber for femtosecond mode-locked erbium-doped fiber laser," Chin. Phys. B **27**, 114214 (2018).
35. L. Hou, Q. M. Lin, Y. G. Wang, Z. D. Chen, J. Sun, H. Y. Guo, Y. Bai, H. W. Chen, B. L. Lu, and J. T. Bai, "Femtosecond ytterbium-doped fiber laser mode-locked by carboxyl-functionalized graphene oxide saturable absorber," Appl. Phys. Express **11**, 012702 (2018).
36. T. J. Wang, J. Wang, Y. G. Wang, X. G. Yang, S. C. Liu, R. D. Lv, and Z. D. Chen, "High-power passively *Q*-switched Nd:$GdVO_4$ reflective graphene oxide saturable absorber," Chin. Opt. Lett. **17**, 020009 (2019).
37. Z. T. Du, H. Wu, T. Q. Zhang, Z. D. Xie, Y. Y. Lv, X. J. Lv, J. L. Xu, G. Zhao, and S. N. Zhu, "Ultra-broadband enhanced nonlinear saturable absorption for $Mo_{0.53}W_{0.47}Te_2$ nanosheets," Chin. Opt. Lett. **18**, 021902 (2020).
38. H. Zhang, D. Y. Tang, X. Wu, and L. M. Zhao, "Multi-wavelength dissipative soliton operation of an erbium-doped fiber laser," Opt. Express **17**, 12692 (2009).
39. B. Guo, Y. Yao, P. G. Yan, K. Xu, J. J. Liu, S. G. Wang, and Y. Li, "Dual-wavelength soliton mode-locked fiber laser with a WS_2-based fiber taper," IEEE Photon. Technol. Lett. **28**, 323 (2016).
40. D. Mao and H. Lu, "Formation and evolution of passively mode-locked fiber soliton lasers operating in a dual-wavelength regime," J. Opt. Soc. Am. B **29**, 2819 (2012).